Design of a 2-axis thrust stand for thrust vectoring diagnostics of an ECR thruster

Etienne Gourcerol, Victor Désangles, Denis Packan, Freddy Gaboriau

DOI: 10.13009/EUCASS2023-731
Aerospace Europe Conference 2023 – 10TH EUCASS – 9TH CEAS

Design of a 2-axis thrust stand for thrust vectoring diagnostics of an ECR thruster

*Etienne Gourcerol**§†, Victor Désangles*, Denis Packan*, Freddy Gaboriau§*
** ONERA, DPHY-FPA - 6, chemin de la Vauve aux Granges 91120 PALAISEAU*
§ Université Toulouse III Paul Sabatier, LAPLACE - 118, route de Narbonne 31060 TOULOUSE
etienne.gourcerol@onera.fr – victor.desangles@onera.fr – denis.packan@onera.fr – freddy.gaboriau@laplace.univ-tlse.fr
† Corresponding Author

Abstract
The design of a 2-axis thrust stand for thrust vectoring diagnostics of an ECR thruster is presented. The instrument consists in two nulled dual pendulum stages. A mechanical model and the transfer function of a dual pendulum stage are computed to predict the response of the thrust stand. Only the actuation gain can increase the amplitude of the response, but the geometrical parameters and the mass repartition of the thrust stand as well as the rotational stiffness of the pivots can be tuned to increase the signal-to-noise ratios.

Nomenclature

θ	Angular deflection of the thrust stand	rad
k	Rotational stiffness of the strip	N·m
V	Axial load	N
F	Strip transverse load or thrust	N
l_{strip}	Strip length	m
w	Strip width	m
e	Strip thickness	m
I	Second moment of inertia	$N \cdot m \cdot s^{-2}$
E	Strip Young's modulus	Pa
l_{arm}	Thrust stand arm length	m
L	Thrust stand platform length	m
P	Weight	N
H	Horizontal load	N
M	Torque	N·m
g	Standard Earth gravity	$m \cdot s^{-2}$
r_G	Vertical position of the centre of mass	m
k_{tot}	Total stiffness of the thrust stand	N·m
s	Complex frequency	s^{-1}
G_a	Complex amplitude of variable a	$[a]$
C	Thrust stand damping coefficient	$N \cdot m \cdot s^{-1}$
K_d	PID derivative gain	s
K_i	PID integral gain	s^{-1}
K_p	PID proportional gain	1
K_{cap}	Capacitive sensor gain	$V \cdot N^{-1}$
K_{act}	Actuator gain	$N \cdot V^{-1}$

DOI: 10.13009/EUCASS2023-731

1. Introduction

Electric propulsion (EP) has been increasingly used in the past years. Indeed, because of their high specific impulse, electric thrusters need less propellant than chemical thrusters for equivalent missions. Hence, EP is used as a replacement for chemical propulsion or to equip smaller satellites like the new satellite internet constellations. Electric thrusters produce plasma accelerated and ejected by electromagnetic fields at speeds above 10 km/s. Some technologies, like the gridded ion thrusters or the Hall effect thrusters, have been flight-proven for more than 50 years. Others are still prototypes like the ECR thruster, a magnetic nozzle (MN) engine developed at ONERA since the 2010s [1]–[4].

In this technology, a diverging magnetic field is produced by a permanent magnet located upstream of the plasma source, a coaxial cavity. Microwave electric power is deposited in the plasma by electron cyclotron resonance (ECR). The perpendicular heated electrons are accelerated in the diverging magnetic field due to the diamagnetic force. Because of the difference in mobility between the electrons and the ions, an ambipolar electric field is created and accelerates the ions. The ejected plasma beam is quasi-neutral. Hence, no neutralising cathode is necessary, contrary to both flight-proven technologies cited above, simplifying greatly the thruster design. The latest results reported a thrust efficiency of 50% for an optimised 30 W thruster. The same model reached a maximum thrust of 2 mN for 50 W and a specific impulse of 2500 s [5].

Another advantage of this technology is the possibility to deflect the magnetic nozzle for thrust vectoring (TV) applications. This ability is important for a satellite for an easier control of the trajectory and a compensation for the centre of mass drift, and requires up to 10° of control [6]. At the moment, a complex and heavy mechanical system is used to move and rotate the thruster assembly. A TV system using only magnetic fields to deflect the MN and the ion beam would reduce the complexity of the whole system. Three types of magnetic vectoring configurations for MN thrusters are reported in the literature and are considered for the TV of the ECR thruster. The first one consists in 1 or 2 transverse coils located on each side of the plasma source that creates a transverse magnetic field [7]–[10]. The second one is a coil winded around the source with a small tilt angle with the thruster axis [11], [12]. The last one consists in two axial coils located on each side of the source that create magnetic fields of opposed directions but parallel to the thruster axis [13].

Most results reported are measurements in the thruster plume including ion saturation current, ion beam current or dynamic momentum flux. These results reveal a deflection of the plume due to the TV system but no quantitative value for the deflection angle. Only one article includes direct thrust measurements of the axial and transverse thrust components measured successively and reports a vectoring angle of 7° for the first type of magnetic vectoring [9]. Therefore, direct and simultaneous measurements of the axial and transverse components of the thrust would increase the confidence in the results and allow for an accurate comparison of the different magnetic vectoring types.

Direct thrust measurements are performed on thrust stands (TS). For EP testing, TS consist in a pendulum arm on which the thruster is attached. While firing, the pendulum displacement is measured. The real thrust value is estimated with a calibration coefficient measured before and/or after firing. Three main configurations are used for the TS: hanging or direct pendulum, inverted pendulum and torsional pendulum [14]. The choice between each configuration is often dictated by internal constraints such as the required sensitivity (displacement per unit of thrust), the size of the vacuum chamber or the specificities of the thruster.

It is possible to combine two direct pendulums into a dual pendulum, which has the geometry of a deformable parallelogram. Both vertical parts, the arms, are free and may tilt. One horizontal part is fixed, the other one is free. The thruster is attached to the second one, called the platform. This geometry main advantage over a simple pendulum is that the equilibrium position does not depend on the mass repartition on the moving platform of the parallelogram. Hence, thermal expansion of this piece, including the thruster, should not affect the measurement. Its main disadvantage is its significant mass, particularly the mass of the platform which is the farthest possible from the fixed axis of rotation. This greatly increases the gravity torque and reduces the sensitivity of the instrument. This kind of TS is used at the Australian National University for studies on RF plasma thrusters and at the Imperial Plasma Propulsion Laboratory in collaboration with the European Space Agency [15], [16]. Both TS operate for thrusters in the mN range with a 10% and 3% standard uncertainty respectively.

The majority of TS measures one component of the thrust vector, but a few 2-axis TS have been the subject of publications. *Nagao et al.* [17] developed a 2-axis direct pendulum using cross-over knife edges and *Duchemin et al.* [18] used a 2-axis TS with a dual pendulum configuration to measure the TV of a Hall effect thruster. *Gilpin et al.* [19] demonstrated the functioning of a 2-axis torsional TS to measure the axial thrust and the mass loss of the thruster simultaneously. Their results were convincing for the µN scale but with limited operating time of a few hours because of flex-pivot bearing thermal drifts. However, these drifts should not affect measurements in the mN scale.

In this article, a 2-axis TS concept with two dual pendulum stages is presented. For the first axis, a mechanical model is solved numerically and the transfer function is computed. The design and possible limitations of each axis are described.

DOI: 10.13009/EUCASS2023-731

2. Thrust stand concept

The 2-axis TS consists in two nulled dual pendulum stages. The first stage (or upper stage) measures the axial thrust and the second stage (or lower stage) the transverse thrust. The 2nd stage is attached to the first one.

2.1 Static resolution of a dual hanging pendulum mechanical model

A mechanical model of a dual hanging pendulum is developed. The hypotheses are:

- Movement are only in the direction of thrust, transverse and torsional movements are neglected,
- Both the arms and the moving platform have a null thickness so that the position of their centre of mass is a function of only one variable: y_1 and y_2 for the arms and x_p for the platform, as described in Figure 1.
- Small deflections: $\theta \ll 1$ so $\sin\theta \sim \theta$ and $\cos\theta \sim 1$,
- Every linkage is a pivot that consists in two spaced strips behaving like deflecting beams under axial load.

The rotational stiffness of a strip subjected to an axial load $V > 0$, is [20]:

$$k(V) = V l_{strip} \times \frac{\cosh(\gamma l_{strip})}{\cosh(\gamma l_{strip}) - 1} \tag{1}$$

where $\gamma = (V/EI)^{1/2}$, l_{strip} is the strip length, E its Young's modulus and $I = we^3/12$ the second moment of inertia, with w the strip width and e its thickness. Thus, for the same transverse load, the higher the axial load, the higher the rotational stiffness and the smaller the beam deflection as described in Figure 2. Hence, the repartition of mass for this TS geometry does have an impact on the stiffness of each pivot. But out of geometrical constraint, each pivot should have the same deflection.

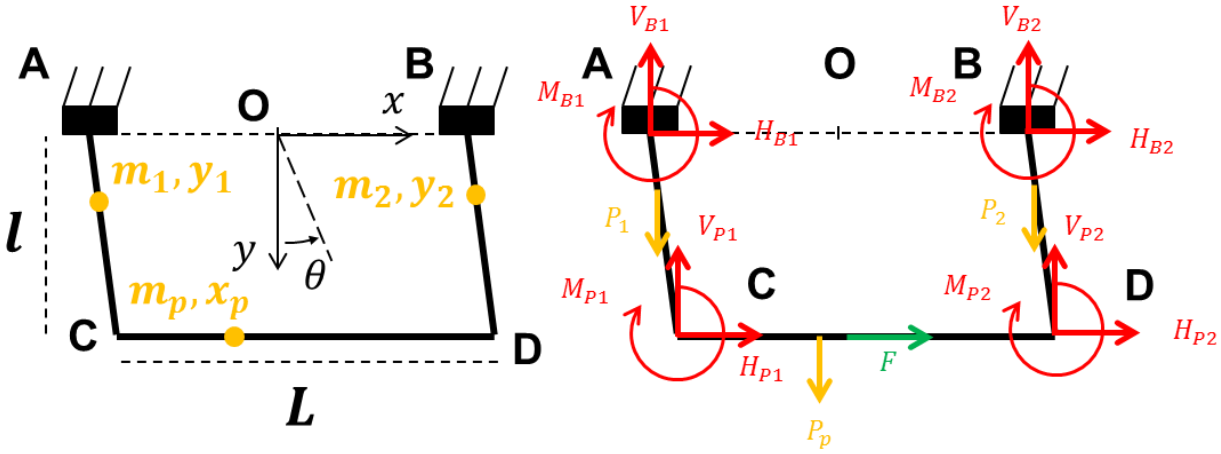

Figure 1: Mechanical system of a dual hanging pendulum thrust stand. The orange dot represents the centre of mass of each component. A and B are fixed. All linkages are pivots behaving like deflecting beams. The thrust force F is applied on the moving platform $\{P\}$ between C and D.

The mechanical system described in Figure 1includes two arms $\{1, 2\}$, one platform $\{P\}$ and one fixed part $\{B\}$. The lengths of the platform and of the arms are L and $l = l_{arm} + 2l_{strip}$ respectively. The thrust force F is applied on the platform. P_i is the weight of the component i. V_{ij}, H_{ij} and M_{ij} are the vertical load, the horizontal load and the torque of component i on component j at the pivot linkage. By isolating one by one the arms and the platform, the following system of equations is found:

Arm 1:

$$\begin{cases} V_{B1} + V_{P1} = P_1 \\ H_{B1} + H_{P1} = 0 \\ A: \; M_{P1} - y_1\theta P_1 + l\,\theta V_{P1} + l\,H_{P1} + M_{B1} = 0 \end{cases} \tag{2}$$

Arm 2:

$$\begin{cases} V_{B2} + V_{P2} = P_2 \\ H_{B2} + H_{P2} = 0 \\ B: \; M_{P2} - y_2\theta P_2 + l\,\theta V_{P2} + l\,H_{P2} + M_{B2} = 0 \end{cases} \tag{3}$$

DOI: 10.13009/EUCASS2023-731

Platform:

$$\begin{cases} V_{1P} + V_{2P} = P_p \\ H_{1P} + H_{2P} + F = 0 \\ C: M_{1P} - \left(\frac{L}{2} + x_p\right) P_p + L V_{2P} + M_{2P} = 0 \end{cases} \quad (4)$$

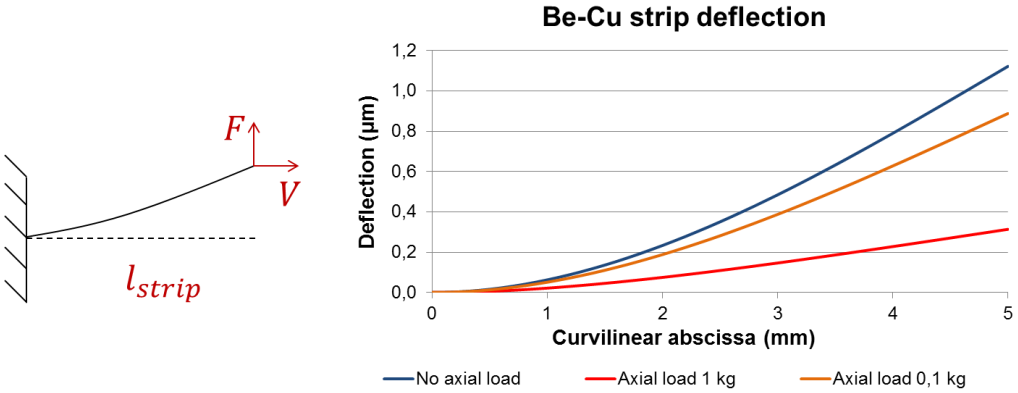

Figure 2: Be-Cu strip deflection under axial load V and transverse load F based on Eq. (1). The strips material is Beryllium-Copper, so $E = 132$ GPa, and the strips dimensions are $l_{strip} = 5$ mm, $w = 5$ mm and $e = 0.1$ mm. $F = 1$ mN.

We have $M_{ij} = -M_{ji} = -2 \times k_{ij}(V_{ij}) \times \theta$ with $i = P, B$ and $j = 1, 2$. The system can be solved analytically for $F = 0$ and numerically for $F \neq 0$ to get θ and all the vertical and horizontal loads. On Figure 3, the deflection $l\theta$ of the TS is plotted in function of the thrust applied to the platform. The geometrical parameters for the simulation are $y_1 = 4$ mm, $y_2 = 4$ mm, $x_p = -10$ mm, $l = 15$ cm, $L = 19$ cm and $m_1 = m_2 = m_p = 4$ kg. The strips material is Beryllium-Copper, so $E = 132$ GPa, and the strips dimensions are $l_{strip} = 5$ mm, $w = 5$ mm and $e = 0.1$ mm. The TS response is linear and the slope is the sensibility $S = 3.11$ µm/mN. It appears that:

$$S = \frac{l^2}{k_{tot}} \quad (5)$$

with $k_{tot} = k_{strips} + k_{mass} = \sum k_{ij} + (y_1 P_1 + y_2 P_2 + l P_p)$, the total stiffness. So this dual pendulum has the same response as a simple hanging pendulum of rotational stiffness $k = k_{strips}$ and mass stiffness $Mgr_G = k_{mass}$ with the thruster and the measurements located at a distance l from the rotation axis [14].

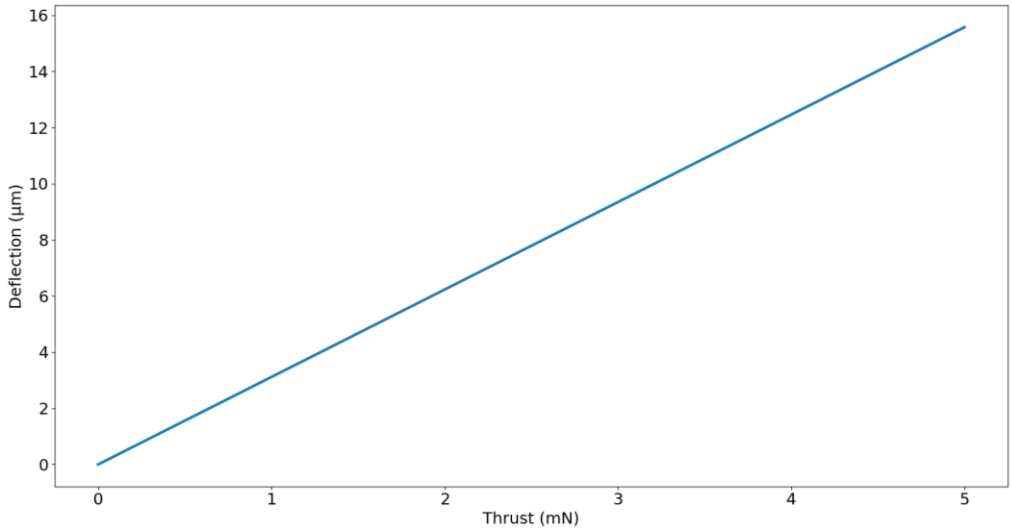

Figure 3: Platform deflection of the dual pendulum in response to a constant thrust. Geometrical parameters for the simulation: $y_1 = 4$ mm, $y_2 = 4$ mm, $x_p = -10$ mm, $l = 15$ cm, $L = 19$ cm and $m_1 = m_2 = m_p = 4$ kg. The Be-Cu strips dimensions: $l_{strip} = 5$ mm, $w = 5$ mm and $e = 0.1$ mm and Young's modulus $E = 132$ GPa .

DOI: 10.13009/EUCASS2023-731

2.2 Transfer function of one axis

The complete system for one axis is presented in Figure 4 as a block diagram. When the thruster is firing, a thrust F is produced at a distance $l_T = l$ from the axis of rotation. The response of the pendulum is described by G_θ/G_M, the transfer function of the pendulum from a torque $M = lF$ to a deflection angle θ:

$$\frac{G_\theta}{G_M}(s) = \frac{1}{k_{tot}} \frac{1}{1 + s\frac{C}{k_{tot}} + s^2\frac{I}{k_{tot}}} \tag{6}$$

with I the moment of inertia of the pendulum, C the damping coefficient and s the complex frequency. G_θ and G_M are the complexe amplitude of θ and $M = lF$. A TS is a low-pass filter. The deflection is measured by the capacitive sensor with a gain $K_{cap}[V/m]$ on the platform, so at a distance $l_{cap} = l$ from the axis of rotation. The output voltage of the sensor is used as input for the PID controller with a transfer function:

$$PID = \frac{V_{PID}}{V_{capa}} = K_d s + \frac{K_i}{s} + K_p \tag{7}$$

with K_p, K_d and K_i the proportional, the derivative and the integral gains respectively. V_{PID} is used as input for the coil/magnet actuator with a gain K_{act} $[N/V]$. The actuator creates an actuation force at a distance $l_{act} = l$ from the axis of rotation opposing the thrust torque.

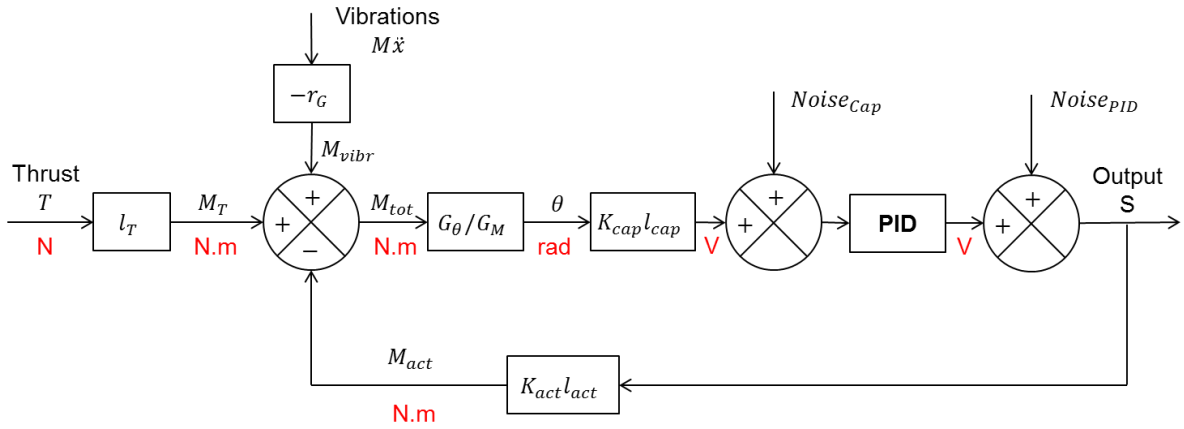

Figure 4: Block diagram of the nulled dual pendulum thrust stand.

The transfer function of the nulled dual pendulum without noises or vibrations:

$$\frac{V_{PID}}{T} = \frac{l_T}{K_{act}l_{act}} \times \frac{1 + s\frac{K_p}{K_i} + s^2\frac{K_d}{K_i}}{1 + s\left(\frac{1}{K_2} + \frac{K_p}{K_i}\right) + s^2\left(\frac{C}{k_{tot}K_2} + \frac{K_d}{K_i}\right) + s^3\frac{J}{k_{tot}K_2}} \tag{8}$$

with $K_2 = k_{tot}(K_i K_{act} K_{cap} l^2)^{-1}$. The system is a first order low-pass filter with a static gain K_{act}^{-1} that does not depend on the dual pendulum geometry. Indeed, we have $l_T = l = l_{act}$. If we consider different sources of noise like the horizontal structure vibrations or the electronic noise from the capacitive sensor or the PID controller, we can compute different signal-to-noise ratio at low frequencies:

$$SNR_{vibrations} = \frac{l}{r_G} \tag{9}$$

$$SNR_{cap} = \frac{K_{act}K_{cap}l^2}{k_{tot}} \tag{10}$$

$$SNR_{PID} = \frac{K_i K_{act} K_{cap} l^2}{k_{tot}} s \tag{11}$$

DOI: 10.13009/EUCASS2023-731

Thus, increasing the length of the arms l, reducing the total stiffness $k_{strips} + k_{mass}$ or the distance of the centre of gravity to the fixed rotation axis r_G will increase the various signal-to-noise ratios. In terms of design, one should have the longest arms possible, the less stiff strips possible, counterweights located above the fixed axis of rotation to compensate for the mass placed below and the smallest overall mass possible. A trade-off should be made for the actuator gain K_{act} as increasing it would increase the signal-to-noise ratios of the PID and the capacitive sensor but would also reduce the static gain of the system.

2.3 Thrust stand design

Both stage are of similar design and consist in two arms and one platform. The designs for the 1-axis and 2-axis TS are presented in Figure 5.A and Figure 5.B respectively. The four pivots located consist in two Be-Cu strips of changeable dimensions. The two strips are 175 mm and 90 mm apart for the 1st and the 2nd stage respectively. Having spaced strips should reduce the magnitude of any parasitic torsional movement around the central axis that could appear due to TV or misalignment. Each stage incorporates a target for a capacitive sensor FOGALE MC900 that measures the displacement of the stage platform. An eddy current damper limits the pendulum oscillations. A coil/magnet actuator is used to maintain a nulled stage displacement with the PID controller described in *Vialis et al.* [21].
For the calibration, small weights are successively deposited on a comb fixed on one arm. The deposition of a weight m at a distance l_m from the arm results in an equivalent known thrust $F_{eq} = l_m l^{-1} mg$ on the platform that creates a measurable response of the PID controller and enables the computation of a calibration coefficient. During the TS operations, V_{PID} is measured and the trust estimated with the calibration coefficient.
HONEYWELL QA 700 accelerometers, actuators and small counterweights are used to level the top fixed part and put the arms in an upright position. Larger counterweights are located on the arms above the top pivot to control the vertical position of their centre of mass. All the arms are 15 cm long.
The 1st and 2nd axis will be used to measure the axial thrust and the transverse thrust with a targeted resolution of 10 µN and 1 µN respectively. Hence, for a 500 µN total thrust, a 0.1° resolution in the vectoring angle measurement is expected. This expected angular resolution should be enough for an accurate comparison of the various TV systems.

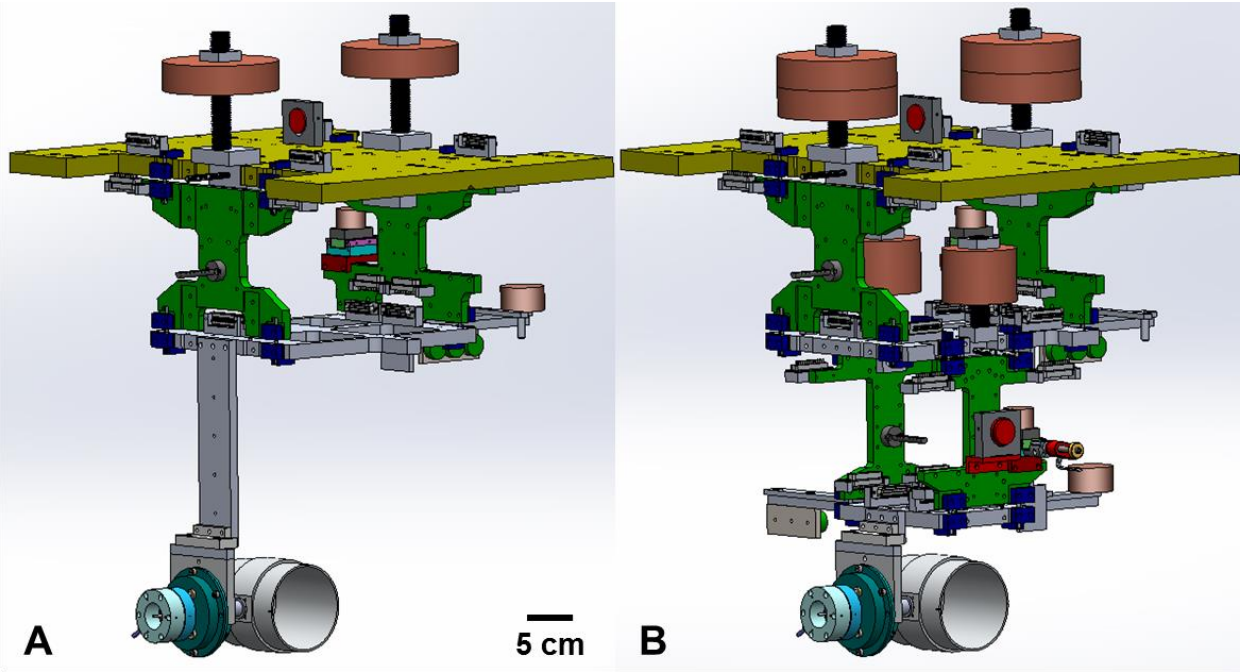

Figure 5: CAD model of the thrust stand concept. A) 1-axis dual pendulum TS. B) 2-axis TS. Yellow: Fixed platform. Blue: Be-Cu strips and fastening. Green: Arms with counterweights above the fixed pivots, one accelerometer per stage and one actuator. The calibration comb is also visible. Grey: Moving platform with capacitive sensor target and magnets for the damping and the actuation. The ECR thruster is at the bottom.

DOI: 10.13009/EUCASS2023-731

The TS will be usable in a 2-axis configuration and in a 1-axis configuration by removing the 2nd stage. Possible limitations will be tested with one axis to confirm the design of the 2nd axis:

- The rotational stiffness of the strips is higher in the transverse direction than in the axial direction by a factor $w^2/e^2 = 2.5 \times 10^3$ in the simulation presented above. Thus, the deflection of the 2nd axis in the axial direction should not be significant.
- The torsional stiffness is expected to be really high so that no torsional movement will take place, because of the significant spacing between the strips. Furthermore, all forces exerted on the platforms will be centred.

3. Conclusion

A 2-axis TS with two dual pendulum stages has been designed for thrust vectoring diagnostics of an ECR thruster. It was shown that the response of the 1-axis dual pendulum is the one of a simple hanging pendulum of equivalent centre of mass position and of total stiffness. The computation of the transfer function of the nulled 1-axis TS highlighted the role of the various parameters for the signal-to-noise ratios: length of the arms, vertical position of the centre of mass, total mass and total stiffness.
Based on these preliminary calculations, a 2-axis TS design was suggested. It consists in two dual pendulum stages, the first one deflecting in response to the axial thrust and the second one in response to the transverse thrust. Both stages displacements are controlled with a capacitive sensor and a coil/magnet actuator.
In the coming months, the torsional stiffness and the rotational stiffness in the transverse directions of the strips will be measured to ensure the absence of significant torsional or transverse movements. The 1-axis dual pendulum configuration will be used to measure successively the axial and transverse thrusts of the ECR thruster with a TV system. These measurements will be used to validate the 2-axis TS design before its fabrication.

References

[1] F. Cannat, ‘Caractérisation et modélisation d’un propulseur plasma à résonance cyclotronique des électrons’, Ecole polytechnique, 2015.
[2] T. Vialis, ‘Développement d’un propulseur plasma à résonance cyclotron électronique pour les satellites’, Sorbonne Université, 2018.
[3] S. Peterschmitt, ‘Development of a Stable and Efficient Electron Cyclotron Resonance Thruster with Magnetic Nozzle’, Institut Polytechnique de Paris, 2020.
[4] F. Boni, ‘Development of a microwave plasma diagnostic applied to electric propulsion systems’, These de doctorat, université Paris-Saclay, 2022.
[5] V. Désangles *et al.*, ‘ECRA thruster advances: 30W and 200W prototypes latest performances’, *Journal of Electric Propulsion*, vol. 2, Mar. 2023, doi: 10.1007/s44205-023-00046-x.
[6] D. G. Fearn, ‘Ion Thruster Thrust Vectoring Requirements and Techniques’, presented at the 27th International Electric Propulsion Conference, Pasadena, CA, USA, Oct. 2001, p. 18.
[7] C. Charles, R. W. Boswell, W. Cox, R. Laine, and P. MacLellan, ‘Magnetic steering of a helicon double layer thruster’, *Applied Physics Letters*, vol. 93, no. 20, 2008, doi: 10.1063/1.3033201.
[8] W. Cox, C. Charles, R. W. Boswell, R. Laine, and M. Perren, ‘Magnetic Ion Beam Deflection in the Helicon Double-Layer Thruster’, *Journal of Propulsion and Power*, vol. 26, no. 5, pp. 1045–1052, Sep. 2010, doi: 10.2514/1.49202.
[9] R. Imai and K. Takahashi, ‘Demonstrating a magnetic steering of the thrust imparted by the magnetic nozzle radiofrequency plasma thruster’, *Appl. Phys. Lett.*, vol. 118, no. 26, p. 264102, Jun. 2021, doi: 10.1063/5.0058202.
[10] R. Imai and K. Takahashi, ‘Deflections of dynamic momentum flux and electron diamagnetic thrust in a magnetically steered rf plasma thruster’, *J. Phys. D: Appl. Phys.*, vol. 55, no. 13, p. 135201, Mar. 2022, doi: 10.1088/1361-6463/ac4451.
[11] A. Caldarelli, F. Filleul, C. Charles, R. Boswell, N. Rattenbury, and J. Cater, ‘Radial characterization of an ion beam in a deflected magnetic nozzle’, *J Electr Propuls*, vol. 1, no. 1, p. 10, Sep. 2022, doi: 10.1007/s44205-022-00012-z.
[12] M. Merino and E. Ahedo, ‘Contactless steering of a plasma jet with a 3D magnetic nozzle’, *Plasma Sources Science and Technology*, vol. 26, no. 9, 2017, doi: 10.1088/1361-6595/aa8061.

DOI: 10.13009/EUCASS2023-731

[13] K. Takahashi and R. Imai, ‘Two-dimensional deflection of a plasma plume exhausted from a magnetically steered radiofrequency plasma thruster’, *Physics of Plasmas*, vol. 29, no. 5, 2022, doi: 10.1063/5.0090476.
[14] J. E. Polk *et al.*, ‘Recommended Practice for Thrust Measurement in Electric Propulsion Testing’, *Journal of Propulsion and Power*, vol. 33, no. 3, pp. 539–555, May 2017, doi: 10.2514/1.B35564.
[15] A. Schwertheim, E. Rosati Azevedo, G. Liu, E. Bosch Borràs, L. Bianchi, and A. Knoll, ‘Interlaboratory validation of a hanging pendulum thrust balance for electric propulsion testing’, *Review of Scientific Instruments*, vol. 92, no. 3, p. 034502, Mar. 2021, doi: 10.1063/5.0037100.
[16] S. Pottinger, V. Lappas, C. Charles, and R. Boswell, ‘Performance characterization of a helicon double layer thruster using direct thrust measurements’, *J. Phys. D: Appl. Phys.*, vol. 44, no. 23, p. 235201, Jun. 2011, doi: 10.1088/0022-3727/44/23/235201.
[17] N. Nagao, S. Yokota, K. Komurasaki, and Y. Arakawa, ‘Development of a two-dimensional dual pendulum thrust stand for Hall thrusters’, *Review of Scientific Instruments*, vol. 78, no. 11, p. 115108, Nov. 2007, doi: 10.1063/1.2815336.
[18] O. Duchemin *et al.*, ‘Testing of a Thrust Steering Device on the PPS®1350 Hall Thruster’, in *42nd AIAA/ASME/SAE/ASEE Joint Propulsion Conference & Exhibit*, Sacramento, California: American Institute of Aeronautics and Astronautics, Jul. 2006. doi: 10.2514/6.2006-4478.
[19] M. R. Gilpin, W. A. McGehee, N. I. Arnold, M. R. Natisin, and Z. A. Holley, ‘Dual-axis thrust stand for the direct characterization of electrospray performance’, *Review of Scientific Instruments*, vol. 93, no. 6, p. 065102, Jun. 2022, doi: 10.1063/5.0087716.
[20] R. J. Roark, W. C. Young, and R. G. Budynas, *Roark’s formulas for stress and strain*, 7th ed. New York: McGraw-Hill, 2002.
[21] T. Vialis, J. Jarrige, A. Aanesland, and D. Packan, ‘Direct Thrust Measurement of an Electron Cyclotron Resonance Plasma Thruster’, *Journal of Propulsion and Power*, vol. 34, no. 5, pp. 1323–1333, Sep. 2018, doi: 10.2514/1.B37036.